Polaron spin echo envelope modulations in an organic semiconducting polymer

V. V. Mkhitaryan and V. V. Dobrovitski

Polaron spin echo envelope modulations in an organic semiconducting polymer

V. V. Mkhitaryan and V. V. Dobrovitski*

Ames Laboratory, Iowa State University, Ames, Iowa 50011, USA

We present a theoretical analysis of the electron spin echo envelope modulation (ESEEM) spectra of polarons in a semiconducting π- conjugated polymers. We show that the contact hyperfine coupling and the dipolar interaction between the polaron and the proton spins give rise to different features in the ESEEM spectra. Our theory enables direct selective probe of different groups of nuclear spins which affect the polaron spin dynamics. Namely, we demonstrate how the signal from the distant protons (coupled to the polaron spin via dipolar interactions) can be distinguished from the signal coming from the protons residing on the polaron site (coupled to the polaron spin via contact hyperfine interaction). We propose a method for directly probing the contact hyperfine interaction, that would enable detailed study of the polaron orbital state and its immediate environment. We also analyze the decay of the spin echo modulation, and its connection to the polaron transport.

I. INTRODUCTION

Over the past decades, semiconducting organic π- conjugated small molecule and polymer materials have been become widely used in optoelectronic devices such as light-emitting diodes and solar cells.[1,2] This triggered an increasing interest in the area of organic electronics, uncovering a variety of new concepts. Remarkably, it was established that the charge carrier spin is fundamental to electrical and optical properties of organic semiconductors. However, because of the extremely complex nature, many important aspects of the spin dynamics and underlying microscopic mechanisms are not yet well understood. This includes the microscopic structure of charge-carrier polaron states, and the resulting hyperfine coupling of polaron spin to the local magnetic environment, which is a key for understanding the spin-dependent processes in organic semiconductors.

Optically and electrically detected magnetic resonance (ODMR and EDMR, respectively) are highly efficient spectroscopic tools for the investigation of microscopic properties of organic semiconductors.[3] While the conventional electron spin resonance (ESR) techniques measure the spin polarization, ODMR and EDMR probe optically and electrically active paramagnetic states,[4–6] which are crucial to many organic semiconductor applications. Moreover, as the spin polarization in organic semiconductors is typically low, ODMR and EDMR are much more sensitive than the conventional ESR.[7–9]

Substantial progress in this direction was made by the pulsed EDMR (pEDMR) experiments.[10–16] Unlike the continuous wave measurements, these experiments are capable of probing the coherent spin dynamics, and thus provide a closer view on the spin-dependent processes. Importantly, pEDMR (and pODMR) offer the implementation of various spin-echo based spectroscopic techniques in the study of organic semiconductors.[14,15] This motivates the present theoretical study of a spectroscopic method based on the two-pulse (Hahn) echo and three-pulse echo sequences.[17]

In many organic semiconductors the spin-orbital coupling is very weak, and the polaron spin dynamics is governed mainly by the hyperfine interaction (HFI) of the polaron spin with the surrounding proton spins.[18,19] Therefore, probing the polaron's HFI is very important. In particular, electron spin echo envelope modulation (ESEEM) spectroscopy[20,21] is a very informative magnetic resonance technique that is widely used for investigation of the hyperfine interactions of paramagnetic centers. The pEDMR implementation of this technique, applied to organic polymer poly[2-methoxy-5-(2′-ethyl-hexyloxy)- 1,4-phenylene vinylene] (MEH-PPV), was recently reported by Malissa et al.[15] Employing a version of ESEEM, the authors of Ref. 15 have been able to resolve the proton spectral line in MEH-PPV and the deuteron and the proton lines in partially deuterated MEH-PPV.

In this paper we develop a theory of ESE modulations in organic semiconducting polymers for two most common pulse experiments, the two-pulse primary echo, and the three-pulse stimulated echo (corresponding to primary and stimulated ESEEM, respectively). Our theory enables direct selective probe and investigation of different groups of nuclear spins which affect the polaron spin relaxation. For instance, we show that, by appropriately choosing the experimental parameters, it is possible to selectively measure the signal from the distant protons (coupled to the polaron spin via dipolar interactions) and distinguish it from the signal coming from the protons residing on the polaron site (coupled to the polaron spin via contact HFI). Based on our theoretical analysis, we conclude that the spectral lines observed in Ref. 15 come from the distant protons, while the same-site protons are not detected. We propose a method for directly probing the contact HFI, that would enable detailed study of the polaron orbital state and its immediate environment.

The paper is organized as follows. In the next Section we discuss the hyperfine interaction between the polaron and the proton spins, particularly in polymer poly[p-phenylene vinylene] (PPV) and its derivative, MEH-PPV. The analytical description of ESEEM is given in Section III. In Section IV we analyze the effect of random orientations of the polymer chains. The polaron hopping and the resulting ESE modulation decay is considered in Section V. We discuss our results in Section VI. Appendices contain the details of our analytical and

numerical calculations.

II. POLARON SPIN IN A π- CONJUGATED ORGANIC SEMICONDUCTING MATERIAL

The polarons in organic semiconductors reside on certain molecular or polymer sites and hop between the sites. While residing on a site the polaron spin $\mathbf{S}$ interacts with N surrounding hydrogen nuclear spins $\mathbf{I}_j = 1/2$, $j = 1, .., N$. In a strong static magnetic field $\mathbf{B}_0 = B_0\hat{\mathbf{z}}$ the polaron spin dynamics is described by the Hamiltonian,

$$H = \Omega S^z + \sum_{j=1}^{N} S^z\left(A_j I_j^z + B_j I_j^x\right) - \omega_I \sum_{j=1}^{N} I_j^z, \quad (1)$$

where $\Omega = \gamma_e \hbar B_0$ and $\omega_I = \gamma_n \hbar B_0$ are the polaron and the nuclear Larmor frequencies, respectively, and $\{A_j\}$, $\{B_j\}$ are the coupling constants that correspond, depending on the location of the nuclear spin, either to the contact hyperfine [Eq. (3)] or to the dipole-dipole interaction [Eq. (5)]. This (pseudo)secular description[17] implies that B_0 greatly exceeds the local magnetic fields created by the nuclear magnetic moments, i.e., $\Omega \gg \omega_{\mathrm{hf}}$, where $\omega_{\mathrm{hf}} = \frac{1}{2}\sqrt{\sum_j(A_j^2 + B_j^2)}$ is the average polaron precession frequency in the local field of the surrounding nuclear spins. Assuming measurements in the X – band,[14,15] we will take $B_0 \approx 345$ mT and $\omega_I/2\pi \approx 14.7$ MHz.

The coupling constants in Eq. (1) depend on the relative orientation of $\mathbf{B}_0$ and the polaron host molecular or polymer site. Typically, organic semiconductors are amorphous materials lacking any long range order in molecular or polymer orientations. Thus, the coupling constants $\{A_j, B_j\}$ differ from site to site, even if the sites have the same microscopic structure.

Polarons in conjugated polymer PPV and MEH-PPV

The hyperfine interaction between the polaron and the proton spins is determined by the chemical structure of host molecule or polymer, which also governs the orbital state of the polaron. To be specific, we focus on the polymer PPV and its derivative, MEH-PPV (see Fig. 1). We base our consideration on the picture of the polaron wavefunction and underlying HFI advocated in Refs. 24–27; for a comprehensive review, see Ref. 28.

The protons can be naturally divided into two groups. The first group includes protons located within the envelope of the polaron's orbital wavefunction, thus contributing to the *contact* HFI. These are the protons of the C–H groups covalently coupled to the polymer backbone carbons, where the polaron wavefunction resides. Because of the exponentially fast spatial decay the polaron wavefunction covers a finite number of such protons. As
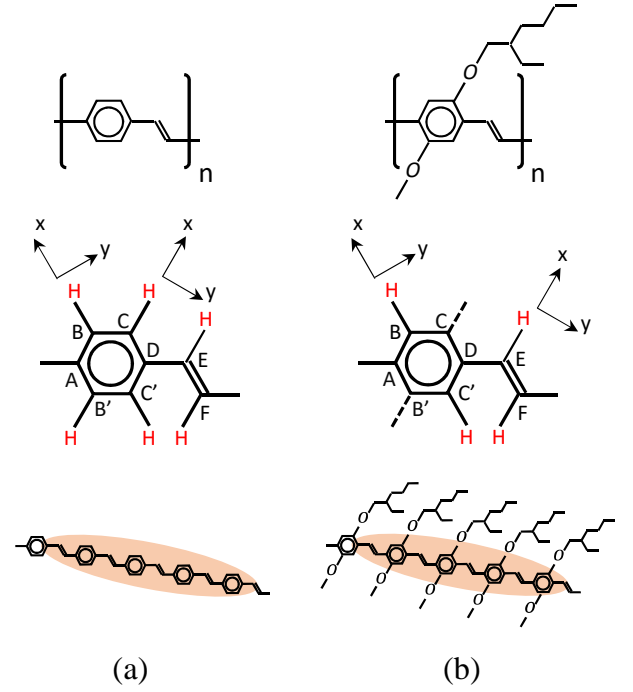

FIG. 1: (Color online) Conjugated polymer PPV (a) and its derivative, MEH-PPV (b). Upper and middle panels show the chemical structures and the unit cells. The principal x, y axes of the C–H proton hyperfine tensors at B and C′ carbon sites are different from those at B′, C, E, and F carbon sites, while the z axes are the same and perpendicular to the plane of the picture (in MEH-PPV there are no C–H protons at B′ and C sites). Lower panels: half-widths of the spatial extents of polarons (orange ovals), according to Ref. 26.

discussed below, in PPV and MEH-PPV this number is order of few tens. Therefore we neglect the contact protons which are coupled to the polaron spin weaker than 0.5 MHz; the number of such contact protons is small, and their overall effect is inessential.

Distant protons, which form the second group, couple to a polaron spin via magnetic dipolar interactions. These protons belong both to polymer backbones and substituent side-groups. Simple estimates show that nearly every distant proton couples to a polaron spin with less than 1 MHz strength. However, because of the slow, $\propto 1/r^3$ decay of the dipolar interaction the effective number of these protons is of the order of few thousand, so that their overall effect can be noticeable, and sometimes even dominant.

1. Contact hyperfine interaction

The polaron spin $\mathbf{S}$ couples to a C–H proton spin $\mathbf{I}$ via the hyperfine interaction $\mathbf{S} \cdot \rho_{\mathrm{S}} \hat{\mathbf{A}} \cdot \mathbf{I}$, where ρ_{S} is the polaron spin density on the carbon $p\pi$ orbital and $\hat{\mathbf{A}}$ is the hyperfine tensor. Thus the polaron contact hyperfine interaction is completely described in terms of $\hat{\mathbf{A}}$ and ρ_{S}.

From the analysis of unpaired carbon orbital states it was established[29] that the principal x and z axes of the hyperfine tensor are parallel to the C–H bond and the $p\pi$ orbital axes, respectively (see Fig. 1). Principal elements of the hyperfine tensor are approximately expressed as

$$\left(A_x, A_y, A_z\right) = -\left([1 - \alpha]A_H, [1 + \alpha]A_H, A_H\right), \quad (2)$$

where $A_H/2\pi = 60$ to 80 MHz is the McConnell's constant, and $\alpha = 0.5$ to 0.6 is the degree of anisotropy.[29]

Equation (2) is quite generally applicable to organic π-electron radicals. For PPV and MEH-PPV, the experimental studies suggest $A_H/2\pi = 70$ MHz and $\alpha = 0.5$.[24–26] These numerical values are used in our calculations. The remaining ingredient needed for description of the polaron contact HFI is the polaron spin density at the carbon sites, ρ_S. In our subsequent calculations we use the spin density presented in Table I. The numbers presented there have been obtained from a model calculation,[27] and have been verified by the analysis of spectral lineshapes in ENDOR[24,25] and light-induced ESR[26] experiments.

Formally, ρ_S in Table I is calculated for PPV. However, the same data can be used for other PPV derivatives,[26] particularly for MEH-PPV, neglecting the effect of substituent groups on ρ_S.

The consideration below is focused primarily on MEH-PPV, since its ESEEM spectra have been studied in Ref. 15. According to Table I and Fig. 1, in MEH-PPV there are $N_c = 22$ contact proton spins coupled to the polaron spin at sites B, C', E, and F, distributed over 7 consecutive unit cells which are covered by the polaron wavefunction (note that in MEH-PPV the C–H protons at carbon sites B and C' are replaced by substituent groups). In the Hamiltonian (1) we label the contact protons by $j = 1, .., N_c$. The coupling constants $\{A_j, B_j\}_{j=1}^{N_c}$ depend on the relative orientations of the corresponding C–H bonds and the applied magnetic field, $\mathbf{B}_0 = B_0\hat{\mathbf{z}}$. We denote the components of $\hat{\mathbf{z}}$ in the principal basis of the j-th hyperfine tensor by $q_{\mu j}$, $\mu = x$, y, z. The

TABLE I: Spin density of a polaron in PPV chain, ρ_S, taken from Ref. 27. Small values, $|\rho_S| < 0.005$, are neglected. The site assignment corresponds to that of Fig. 1. The unit cell at the polaron center is denoted by 0, thereby the unit cells with significant values of ρ_S range from -3 to 3.

site\cell	-3	-2	-1	0	1	2	3
A	–	0.01	0.04	0.08	0.04	–	–
B	–	0.01	-0.015	0.035	-0.005	0.03	-0.005
B'	–	0.01	-0.015	0.04	–	0.03	–
C	–	–	0.03	–	0.04	-0.015	0.01
C'	–	-0.005	0.03	-0.005	0.035	-0.015	0.01
D	–	–	–	0.04	0.08	0.04	0.01
E	0.01	-0.01	0.09	0.08	–	0.035	–
F	–	0.035	–	0.08	0.09	-0.01	0.01

coupling constants are related to the hyperfine tensor elements Eq. (2) as

$$A_j = \rho_S(j)\sum_\mu A_\mu q_{\mu j}^2, \quad A_j^2 + B_j^2 = \rho_S^2(j)\sum_\mu A_\mu^2 q_{\mu j}^2. \quad (3)$$

For each j, $\rho_S(j)$ is given in Table I, and $q_{\mu j}$ can be found for any direction of $\mathbf{B}_0$ from the description of the principal hyperfine axes in Fig. 1. The protons coupled to the polaron via contact HFI create a random local magnetic field. The number of such protons is quite large, so the random field has almost Gaussian probability distribution. From Table I we calculate its standard deviation, $\omega_{\mathrm{hf},c}/\hbar\gamma_e$, where the hyperfine frequency

$$\omega_{\mathrm{hf},c} = \left\langle \frac{1}{2}\sqrt{\sum_{j \le N_c} \left(A_j^2 + B_j^2\right)} \right\rangle \approx 2\pi \times 7.25\,\mathrm{MHz} \quad (4)$$

is an average over the polaron random orientations. The corresponding ESR line would have a Gaussian shape with the full width at half maximum of 6.1 G, in agreement with Ref. 26.

2. Interaction with the distant protons

Distant protons couple to the polaron spin via magnetic dipolar interaction. The strength of this interaction is determined by the material morphology, including the molecular packing and the average density of protons. Relying upon the reported data on the molecular packing[30–32] and van der Waals radii of hydrogen and carbon[33–35], we restrict the minimal distance between the polymer backbone carbons and distant protons to $d_{\min} = 2.2$ Å. Furthermore, based on the MEH-PPV mass density 1 g/mL[31,32] and its chemical structure shown in Fig. 1, we infer the average proton density 55 nm^{-3}. Correspondingly, we assume that the protons are uniformly randomly distributed over the sample with the average density of 55 nm^{-3}, except for the (distant) proton-free cylindrical regions of the radius $d_{\min}$ around the polymer backbone. The polaron spin density, being strongly concentrated around the 38 carbon sites given in Table I, can be approximated as a sum of 38 delta function-like peaks. Therefore, the coupling constants A_j and B_j which describe the dipolar interaction between the j-th distant proton and the polaron spin, include the summation over the 38 point-like regions, i.e.

$$A_j = \hbar\gamma_e\gamma_n \sum_{l=1}^{38} \rho_S(l)\frac{1 - 3\cos^2\theta_{lj}}{R_{lj}^3},$$

$$B_j = \hbar\gamma_e\gamma_n \sum_{l=1}^{38} \rho_S(l)\frac{3\sin\theta_{lj}\cos\theta_{lj}}{R_{lj}^3}. \quad (5)$$

Here, $\rho_S(l)$ is the polaron spin density at the carbon site l, $\mathbf{R}_{lj}$ is the vector connecting the distant proton to this carbon site, and θ_{lj} is the angle between $\mathbf{R}_{lj}$ and $\mathbf{B}_0$.

A large number of distant protons is included in our numerical simulations. The locations of the distant protons are sampled from the distribution described above (uniform, with the exception of the proton-free cylinders around the polymer chains), and the averaging over many different samples is performed. In our simulations the results converge for about $N_d = 2000$ distant protons, and do not change appreciably if this number is increased by an order of magnitude. This is because we deal with spatial integrals of $\sim A^2, B^2$, and their combinations, which vanish as $\propto R^{-6}$ or faster, and thus converge quickly. Averaging over the random orientations of polymer chains should be performed additionally, as the polaron spin density is not spherically symmetric and different chain orientations are inequivalent.

The random local frequencies created by the distant protons will have a typical magnitude of $\omega_{\mathrm{hf},d} \approx 2\pi \times 2$ MHz, leading to the the total linewidth,

$$\omega_{\mathrm{hf}} = \left\langle \frac{1}{2}\sqrt{\sum_{\mathrm{all}\ j}\left(A_j^2 + B_j^2\right)} \right\rangle \approx 2\pi \times 7.52\,\mathrm{MHz}. \qquad (6)$$

From Eqs. (4) and (6) it is seen that, on average, the distant protons are responsible only for a small fraction of the local hyperfine field. Yet they have a strong effect on the fine structure of ESEEM, as will be seen shortly.

Note that the distinction between contact and distant protons is rather sharp, with a well defined d_{min} controlled by the molecular packing. Although for some contact-coupled protons the hyperfine coupling is somewhat weak (comparable to the coupling of the distant protons), the number of such protons is small, and their influence on the spectra is negligible.

In theoretical studies of the spin dynamics in organic semiconductors the semiclassical approach[22] is often used. While this approach does not capture all details of the ESEEM signal, it provides a convenient way for the characterization of signal decay. Within the semiclassical treatment, the nuclear spin dynamics given by the last term of Eq. (1) is ignored, and the on-site hyperfine interaction is replaced by a random local static magnetic field experienced by the polaron spin.[22] Accordingly, the on-site semiclassical Hamiltonian in the secular approximation reads:

$$H_{SC} = \left(\Omega + \omega_z\right)S^z, \qquad (7)$$

where ω_z is random and uncorrelated from site to site. This random frequency is approximately described by the Gaussian distribution, with the standard deviation ω_{hf} [see Eq. (6)]. Note that the distribution of random fields resulting from the bath of dilute spins is Lorentzian, rather than Gaussian,[23] and may provide an alternative description for the distant protons in highly deuterated samples. However, because of moderate dilution of protons even in the deuterated samples and overall small contribution of distant protons to ω_{hf}, the Gaussian distribution of local frequencies is sufficiently accurate for the purposes of our study.
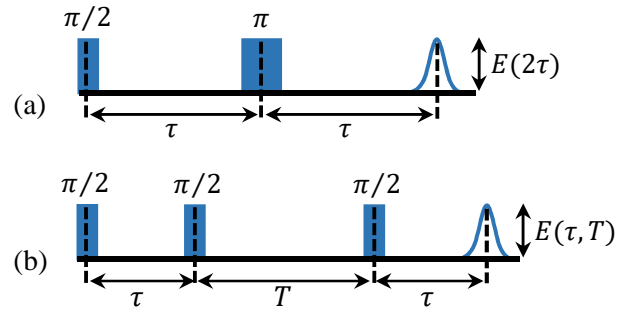

FIG. 2: (Color online) The ESEEM pulse sequences considered in the text. (a) Primary ESEEM. (b) Stimulated ESEEM.

III. SPIN ECHO WITH IDEAL PULSES

Generally, ESEEM spectroscopy is used to investigate the hyperfine interactions of paramagnetic species.[20] To set a framework for discussing the application of spin echo experiments to organic semiconductors, we discuss the ESEEM in the case of the two-pulse Hahn echo sequence, Fig. 2(a) (primary ESEEM), and the three-pulse sequence, Fig. 2(b) (stimulated ESEEM). In Fig. 2, $\pi/2$ and π denote the rotation angle of spins around the x-axis in the rotating frame, induced by resonant microwave pulses, whereas τ and T are the free evolution periods between the pulses. The pulses are assumed to be ideal. Depending on τ and T the echo amplitude, which we denote by $E(2\tau)$ for the primary ESEEM and $E(\tau, T)$ for the stimulated ESEEM, undergoes modulation caused by the coupling to the nuclear spins.

Using the density matrix formalism, the (normalized) echo amplitudes can be written as

$$E(2\tau) = -2\,\mathrm{Tr}\left[U(\tau)\hat{\rho}(0)U^\dagger(\tau)S^y\right], \qquad (8)$$

$$E(\tau, T) = -2\,\mathrm{Tr}\left[U(\tau, T)\hat{\rho}(0)U^\dagger(\tau, T)S^y\right], \qquad (9)$$

where $\hat{\rho}(0)$ is the density operator before the first pulse, and the evolution operators are given by

$$U(\tau) = e^{-i\tau H}\left[\pi\right]e^{-i\tau H}\left[\pi/2\right],$$

$$U(\tau, T) = e^{-i\tau H}\left[\pi/2\right]e^{-iTH}\left[\pi/2\right]e^{-i\tau H}\left[\pi/2\right],$$

where $[\phi] = \exp(i\phi S^x)$ denotes the rotation operator for an ideal pulse with the flip angle ϕ, and H is the Hamiltonian, as given by Eq. (1). We consider the initial density operator $\hat{\rho}(0) = (1/2 + S^z) \otimes \rho_I$ that describes the polaron spin ensemble polarized along the z-axis. We can neglect the thermally-induced polarization of the nuclear spin ensemble and take the nuclear density operator proportional to the unity, $\rho_I \propto \mathbf{1}$. The explicit calculation of modulation functions is facilitated by the fact that the Hamiltonian, Eq. (1), preserves the z-component of polaron spin. One gets[20]

$$E(2\tau) = \prod_{j=1}^{N}\left(1 - 2k_j \sin^2\frac{\omega_{j+}\tau}{2}\sin^2\frac{\omega_{j-}\tau}{2}\right) \qquad (10)$$

for the primary ESEEM and

$$E(\tau, T) = \frac{1}{2} \prod_{j=1}^{N} \left(1 - 2k_j \sin^2 \frac{\omega_{j+}[\tau+T]}{2} \sin^2 \frac{\omega_{j-}\tau}{2} \right)$$
$$+ \frac{1}{2} \prod_{j=1}^{N} \left(1 - 2k_j \sin^2 \frac{\omega_{j+}\tau}{2} \sin^2 \frac{\omega_{j-}[\tau+T]}{2} \right) \quad (11)$$

for the stimulated ESEEM, where the frequencies,

$$\omega_{j\pm} = \left[(\omega_I \pm A_j/2)^2 + B_j^2/4 \right]^{1/2}, \quad (12)$$

are the nuclear spin precession frequencies corresponding to the polaron spin being up $(+)$ and down $(-)$, and

$$k_j = \left[\frac{\omega_I B_j}{\omega_{j+} \omega_{j-}} \right]^2 \quad (13)$$

are the modulation depths.

Two major factors influencing modulation signals Eqs. (10) and (11) in a real experiment are the orientation disorder of the polymer chains and random hopping of the polaron between different sites. In the next two Sections we study the effects of these factors.

IV. THE EFFECT OF ORIENTATION DISORDER

In the typical experiments the samples are the disordered films of the organic polymer, so the observed signals include contributions from all orientations of the polymer chains. Therefore we average Eqs. (10) and (11) over random orientations of the polymer chains, and consider the disorder-averaged modulation signals, $\langle E(2\tau) \rangle$, $\langle E(\tau, T) \rangle$, together with their spectra given by the cosine Fourier transforms,[36] $\tilde{E}(\omega) = \mathcal{F}_\tau[\langle E(2\tau) \rangle]$, $\tilde{E}(\tau, \omega) = \mathcal{F}_T[\langle E(\tau, T) \rangle]$.

A. Orientation-averaged primary ESEEM

The HFI described above leads to small modulation depths, $k_j \ll 1$. Moreover, the sum of all modulations depths, $\kappa = \sum k_j$, is also small. This allows expansion of Eq. (10) in terms of small k_j (for details see Appendix A). We write:

$$E(2\tau) = 1 - \frac{1}{2} \sum_j k_j \Big[1 - \cos(\omega_{j+}\tau) - \cos(\omega_{j-}\tau)$$
$$+ \frac{1}{2} \cos\big([\omega_{j+} - \omega_{j-}]\tau \big) + \frac{1}{2} \cos\big([\omega_{j+} + \omega_{j-}]\tau \big) \Big]. \quad (14)$$

Equation (14) shows that the primary ESEEM spectrum involves four groups of carrier frequencies, $\{\omega_{j\pm}\}$ and $\{\omega_{j+} \pm \omega_{j-}\}$. We also approximate

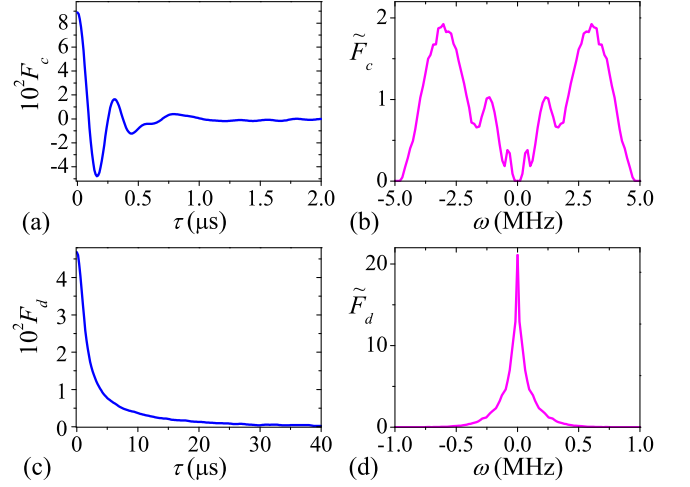$$\omega_{j\pm} \approx \omega_I \pm A_j/2. \quad (15)$$

FIG. 3: (Color online) (a) and (c): the functions $F_c(\tau)$ and $F_d(\tau)$, introduced in Eqs. (17) and (18) respectively, are plotted with blue. (b) and (d): The respective cosine Fourier transforms, $\tilde{F}_c(\omega)$ and $\tilde{F}_d(\omega)$, are plotted with magenta, in the same units.

For the distant protons Eq. (15) follows from the weak coupling, $A_j, B_j \ll \omega_I$. For the contact protons with a stronger coupling Eq. (15) is valid due to the weak anisotropy of the contact HFI, see Appendix A. Equation (15) reveals the four frequency groups in the ESEEM signal, namely $\{|A_j|\}$, $\{\omega_I - |A_j|/2\}$, $\{\omega_I + |A_j|/2\}$, and $2\omega_I$. The relation[37] $\omega_I > \frac{3}{2}|A_j|$ means that the information about $\{|A_j|\}$ is encoded in the low-frequency modulations of the ESEEM signal, which is well separated from the higher frequency groups. Besides, the second and the third groups are close to ω_I, mirroring each other about this frequency.

Another conclusion from Eq. (14) is that the contributions of the contact and the distant protons in $E(2\tau)$ are simply additive. We separate these contributions by introducing the notations, $E_c(2\tau)$ and $E_d(2\tau)$, respectively. More specifically, $E_c(2\tau)$ is the partial sum of the first N_c terms in Eq. (14), whereas $E_d(2\tau)$ includes the terms with $j > N_c$, and thus $E(2\tau) = 1 + E_c(2\tau) + E_d(2\tau)$. Using Eq. (15) in Eq. (14) and averaging the result over the disorder in polymer chain orientations we obtain:

$$\langle E_\beta(2\tau) \rangle = -\frac{\langle \kappa_\beta \rangle}{2} - \frac{1}{4} F_\beta(2\tau) - \frac{\langle \kappa_\beta \rangle}{4} \cos(2\omega_I \tau)$$
$$+ F_\beta(\tau) \cos(\omega_I \tau), \quad (16)$$

where the subscript, $\beta = c, d$, refers to the contact and the distant protons, respectively, and the partial sums

$$F_c(\tau) = \left\langle \sum_{j \le N_c} k_j \cos(A_j \tau/2) \right\rangle, \quad (17)$$

$$F_d(\tau) = \left\langle \sum_{j > N_c} k_j \cos(A_j \tau/2) \right\rangle, \quad (18)$$

with $\kappa_c = \langle \sum_{j=1}^{N_c} k_j \rangle$ and $\kappa_d = \langle \sum_{j > N_c} k_j \rangle$ are introduced. Equation (16) gives the orientation-averaged ESE

modulation function in terms of $F_c(\tau)$ and $F_d(\tau)$. Particularly, the low-frequency modulations are included in the second term of Eq. (16). The third term of Eq. (16) describes oscillations of a constant amplitude at the frequency $2\omega_I$, and includes both the contact and the distant protons. Finally, modulations with the frequencies close to ω_I are incorporated in the last term of Eq. (16).

First we discuss the contribution of distant protons. On the timescale, $\tau \sim 1/\omega_I$, the function $F_d(\tau)$, Fig. 3(c), varies only slightly. Thus the last term of $\langle E_d(2\tau)\rangle$ in Eq. (16) represents oscillations with the frequency ω_I and the envelope $F_d(\tau)$. The cosine Fourier transform, $\tilde{F}_d(\omega)$, plotted in Fig. 3(d), shows a sharp peak at $\omega = 0$. Through this function the cosine Fourier spectrum of the distant protons is described. It involves three well-resolved features; a dip of the form $-\frac{1}{4}\tilde{F}_d(\omega/2)$ near the origin, a sharp peak at ω_I of the shape $\tilde{F}_d(\omega - \omega_I)$, and a sharper negative δ- peak at $2\omega_I$.

In the case of the contact proton contribution, the function $F_c(\tau)$ shown in Fig. 3(a) changes considerably on the timescale $\tau \sim 1/\omega_I$ because of the presence of large $A_j \sim \omega_I$. Therefore, the last term of $\langle E_c(2\tau)\rangle$ in Eq. (16) does not admit a simple interpretation in terms of the oscillations with the frequency ω_I and a smooth envelope. Its cosine Fourier transform, $\tilde{F}_c(\omega - \omega_I)$, incorporates two bands mirroring each other about ω_I, as can be inferred from Fig. 3(b). These bands come from the modes with frequencies $\{\omega_I \pm |A|_j/2\}_{j=1}^{N_c}$, spread by the orientation disorder. Besides these two bands and the negative δ- peak at $2\omega_I$, the cosine Fourier spectrum of contact protons involves a low-frequency band of the form $-\frac{1}{4}\tilde{F}_c(\omega/2)$, originating from the frequencies $\{|A|_j\}_{j=1}^{N_c}$.

Figure 4 plots the primary ESEEM spectrum $\tilde{E}(\omega)$, calculated from Eq. (10) by a Monte Carlo sampling of the polymer chain orientations, employing Eqs. (3), (5). Its structure near $\omega_I = 14.7$ MHz includes a sharp peak at ω_I and two wider side-bands mirroring each other about ω_I. Based on the above analysis, we identify the side-bands with the contribution of contact protons and the sharp peak with the influence of the distant protons. Thus, the shapes of the side-bands and of the sharp peak are given by $\tilde{F}_c(\omega - \omega_I)$ and $\tilde{F}_d(\omega - \omega_I)$, respectively. This identification is clearly confirmed in Fig. 4(b), where we separately plot the contributions of the contact and the distant protons.

B. Orientation-averaged stimulated ESEEM

The stimulated ESEEM can be analyzed along the same lines. Expanding Eq. (11) in terms of small k_j and keeping the leading terms, one gets:

$$E(\tau, T) = 1 - \sum_j \frac{k_j}{2}\left[\sin^2\frac{\omega_{j+}\tau}{2}\left(1 - \cos\omega_{j-}[\tau + T]\right)\right.$$
$$\left. + \sin^2\frac{\omega_{j-}\tau}{2}\left(1 - \cos\omega_{j+}[\tau + T]\right)\right]. \quad (19)$$
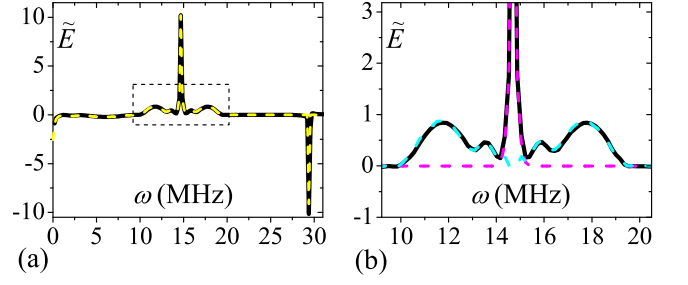

FIG. 4: (Color online) The primary ESEEM spectrum $\tilde{E}$, calculated from orientation disorder averaged Eq. (10) numerically, is plotted in black. (a): The cosine Fourier transform of the sum, $\langle E_c(2\tau)\rangle + \langle E_d(2\tau)\rangle$, is plotted with yellow dashed line, from Eq. (16). (b): Zoom in of the region indicated in the left panel with a rectangle. $\tilde{F}_c(\omega - \omega_I)$ and $\tilde{F}_d(\omega - \omega_I)$ are plotted with the cyan and magenta dotted lines, respectively. It is seen that the spectral peak at $\omega_I = 14.7$ MHz is exclusively due to the distant protons, whereas the side bands come from the contact protons.

Thus, the stimulated ESEEM spectrum involves only two groups of frequencies, $\{\omega_{j+}\}$ and $\{\omega_{j-}\}$. Our subsequent analysis employs the approximation given by Eq. (15). By separating the contact and the distant proton contributions in Eq. (19) and averaging over the polymer chain orientations, we get $\langle E(\tau, T)\rangle = 1 + \langle E_c(\tau, T)\rangle + \langle E_d(\tau, T)\rangle$, where the T- dependent parts of $\langle E_\beta(\tau, T)\rangle$, $\beta = c, d$, are

$$\langle E_\beta(\tau, T)\rangle \simeq \frac{1}{2}F_\beta(\tau + T)\cos(\omega_I[\tau + T]) \quad (20)$$
$$-\frac{1}{4}F_\beta(T)\cos(\omega_I[2\tau + T]) - \frac{1}{4}F_\beta(2\tau + T)\cos(\omega_I T).$$

As a function of T, $\langle E_d(\tau, T)\rangle$ involves only modulations with the proton Zeeman frequency ω_I, and its cosine Fourier transform[36] $\tilde{E}_d(\tau, \omega)$ demonstrates just a sharp peak around that frequency. The τ- dependence of the modulation depth can be understood even without performing the disorder averaging. Indeed, Eq. (19) shows that the modulation amplitude is reduced if τ can be chosen in such a way that $\sin(\omega_{j\pm}\tau/2) \approx 0$ for all protons. Since for the distant protons all $\omega_{j\pm}$ are close to ω_I, one can expect a reduction of the modulation amplitude of $\langle E_d(\tau, T)\rangle$ for the values of τ satisfying $\sin(\omega_I\tau/2) = 0$. Similarly, one can anticipate an increase of the modulation amplitude for the values of τ satisfying the condition $\sin(\omega_I\tau/2) = \pm 1$.

In Appendix A we show that the T- modulation amplitude of $\langle E_d(\tau, T)\rangle$ is reduced when $\tau = \tau_n = (\pi/\omega_I)n$ with even integer n, and increases when n is an odd integer. We also show that, for $n \leq 30$, the difference in the amplitudes of $\langle E_d(\tau_n, T)\rangle$ between odd n and even n is more than two orders of magnitude for small n and more than a factor of 15 for large n. Note that this includes all τ_n within the interval $0 < \tau < 1\,\mu s$, which corresponds to the experimentally plausible values of τ.
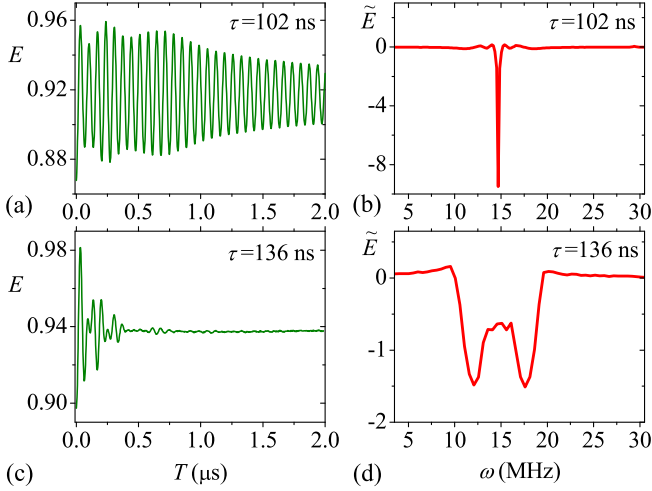
FIG. 5: (Color online) The stimulated ESEEM $\langle E(\tau_n,T)\rangle$, calculated from orientation disorder averaged Eq. (11) numerically, is plotted against T at fixed $\tau_n = (\pi/\omega_I)n$ for $n = 3$, $\tau_3 \approx 102$ ns (a), and $n = 4$, $\tau_4 \approx 136$ ns (c). The corresponding spectra $\tilde{E}(\tau_n,\omega)$, $n = 3$ (b) and $n = 4$ (d), are plotted against ω. The strong reduction of the peak at $\omega_I = 14.7$ MHz for even n, allowing the observation of the contact proton hyperfine coupling, is obvious.

The T- modulation of $\langle E_c(\tau,T)\rangle$ given by Eq. (20) cannot be interpreted as having a single frequency ω_I, because the function F_c varies rapidly on the timescale, $T \sim 1/\omega_I$. Similar to the case of the primary ESEEM, its cosine Fourier transform[36] $\tilde{E}_c(\tau,\omega)$ demonstrates two bands near ω_I. However, in this case these bands are not quite symmetric with respect to ω_I. Importantly, choosing $\tau = \tau_n$ is not critical for $\langle E_c(\tau,T)\rangle$, and there is no reduction of modulation at even n, as shown in Appendix A.

Summarizing, the stimulated ESEEM spectra at $\tau = \tau_n$ with odd n demonstrate a strong peak at ω_I, which could make it difficult to experimentally observe the weaker contact proton sidebands. On the other hand, reduction of the peak occurs at $\tau = \tau_n$ with even n, while the contribution of the contact protons is preserved. This provides a method of distinguishing the signal coming from the distant protons from the modulation caused by the contact protons, coupled to the polaron via HFI.

To illustrate the method, in Fig. 5 we plot the time-domain signals $\langle E(\tau_n,T)\rangle$ along with their spectra for $n = 3$ and $n = 4$, as calculated from the orientation-averaged Eq. (11). The spectra plotted in Figs. 5(b) and (d) demonstrate the suppression of the peak at $\omega_I = 14.7$ MHz when changing n from odd to even.

V. ECHO MODULATIONS OF HOPPING POLARONS

The random hopping of the polaron leads to the decay of ESEEM, thus imposing limitations on the observability of modulations. On the other hand, this decay can serve as a probe for understanding the polaron transport. In this Section we investigate the ESEEM of polarons performing random walk over orientationally disordered polymer sites and coupling to the nuclear spins according to Eq. (1). Our main goal is to reveal the hopping regimes where the ESEEM signal, and particularly the contact hyperfine spectrum, is not distorted.

The spin dynamics of a randomly hopping polaron depends on the dimensionality of the sample.[38–41] Its analytical description is the simplest in 3D, where the self-intersections of the polaron random walk trajectories can be neglected. This is equivalent to the strong collision approximation which provides a simple way of describing the spin relaxation of a randomly hopping carrier.[42]

The multiple trapping model[43–46] is an implementation of the strong collision approximation, often used to explain the transport in organic materials,[47] and particularly in PPV and its derivatives.[48] We base our consideration on the multiple trapping model. Within this model the polaron hopping from a polymer site is described by the rate,

$$W_{\mathbf{r}} = \nu \exp[\varepsilon_{\mathbf{r}}/k_B T], \qquad (21)$$

where ν is the hopping attempt frequency, $\varepsilon_{\mathbf{r}}$ is the trapping energy at the site $\mathbf{r}$, k_B is the Boltzmann constant, and T is the temperature. The trapping energies are all negative and random, with the exponential distribution, $\mathcal{N}(\varepsilon) \propto \exp[\varepsilon/k_B T_0]$. Hence the model is defined by two parameters: the frequency ν and the dispersion parameter $\alpha \equiv T/T_0$. In the high-temperature or shallow-trap limit, when $\alpha \to \infty$, the hopping rates are uniform and the waiting time statistics of the polaron random walk obeys the Poisson distribution, $P(t) = \nu \exp(-\nu t)$. For finite α this distribution assumes the algebraic form, $P(t) \propto t^{-1-\alpha}$, reflecting the broad distribution of the hopping rates.

A. Primary ESEEM of hopping polarons

The generalization of Eq. (10) for hopping polarons and the evaluation of the resulting echo modulation function, $\mathcal{E}(2\tau)$, is described in Appendix B. We calculate $\mathcal{E}(2\tau)$ by Monte-Carlo sampling of the random-walk trajectories over the orientation disordered polymer sites. But before turning to our results on $\mathcal{E}(2\tau)$ we introduce the echo modulation function of hopping carriers calculated from the semiclassical Hamiltonian (7), $\mathcal{E}_{SC}(2\tau)$, which is the semiclassical counterpart of $\mathcal{E}(2\tau)$.

$\mathcal{E}_{SC}(2\tau)$ is a non-oscillatory, monotonously decreasing function of the delay time τ. In the high-temperature

limit, $\alpha \to \infty$, the perturbative treatment over small $\eta \equiv \nu/\omega_{\mathrm{hf}} \ll 1$ given in Appendix C yields

$$\mathcal{E}_{\mathrm{SC}}(2\tau) = \left[1 + \eta\sqrt{\pi}\,\mathrm{erf}(\omega_{\mathrm{hf}}\tau)\right]e^{-2\nu\tau}, \qquad (22)$$

where $\mathrm{erf}(x)$ is the error function. For $\tau > 2/\omega_{\mathrm{hf}}$ the error function in Eq. (22) changes very little, so that $\mathcal{E}_{\mathrm{SC}}(2\tau)$ assumes the exponential form, $\mathcal{E}_{\mathrm{SC}}(2\tau) \propto \exp(-2\tau/T_2)$, with the decoherence time, $T_2 = 1/\nu$. The decay of $\mathcal{E}_{\mathrm{SC}}(2\tau)$ with τ is exponential also in the fast hopping regime, $\eta \gg 1$. However, due to the motional narrowing, the dependence of T_2 on ν in this regime is reversed; $T_2 = \nu/\omega_{\mathrm{hf}}^2$. Combining the two forms, we write:

$$T_2 = 1/\nu + \nu/\omega_{\mathrm{hf}}^2. \qquad (23)$$

Even though the decay of $\mathcal{E}_{\mathrm{SC}}(2\tau)$ in the intermediate regime $\eta \sim 1$ is not exponential, the dephasing time Eq. (23) gives the correct timescale for that decay too.

Our numerical simulations show that with decreasing α the decay of $\mathcal{E}_{\mathrm{SC}}(2\tau)$ becomes slower and non-exponential, with a progressively stronger long-time tail. For $\eta \ll 1$ this can be explained as follows. The dependence of $\mathcal{E}_{\mathrm{SC}}(2\tau)$ on α is stipulated by the number of deep traps, which grows with decreasing α. A trapped polaron is subject to a static hyperfine magnetic field. Because the echo pulse sequence eliminates the dephasing caused by static field components,[17,23] the decay of $\mathcal{E}_{\mathrm{SC}}(2\tau)$ becomes slower with the increasing fraction of trapped polarons. The effect is most pronounced at long times due to the slow, algebraic decrease of the waiting time distribution, resulting in the overall non-exponential dephasing of $\mathcal{E}_{\mathrm{SC}}(2\tau)$.

The dependence of $\mathcal{E}_{\mathrm{SC}}(2\tau)$ on α for $\eta \gg 1$ is less transparent. Nevertheless, the non-exponential character of $\mathcal{E}_{\mathrm{SC}}(2\tau)$ at finite α, observed in our numerical simulations, is established analytically also for this case.[49]

Summarizing, the exponential behavior of $\mathcal{E}_{\mathrm{SC}}(2\tau)$ is a signature of the uniform hopping rates with either fast or slow hopping (i.e., away from $\eta \sim 1$), whereas in all the remaining situations $\mathcal{E}_{\mathrm{SC}}(2\tau)$ is non-exponential.

The analysis of $\mathcal{E}(2\tau)$ reveals different types of τ- dependence in slow ($\eta \ll 1$) and fast ($\eta \gg 1$) hopping regimes. In the slow hopping regime, where this dependence is more complex, we numerically find that $\mathcal{E}(2\tau)$ is quite accurately quantified by

$$\mathcal{E}(2\tau) = \langle E(2\tau)\rangle \mathcal{E}_{\mathrm{SC}}(2\tau), \qquad (24)$$

where $\langle E(2\tau)\rangle$ is established in the previous Section. To substantiate this relation, in Fig. 6 we plot $\mathcal{E}(2\tau)$ numerically calculated for four different small values of η, and compare them with the curves resulting from Eq. (24). The plots confirm the validity of Eq. (24) for the hopping attempt frequencies up to $\eta = 0.21$.

Equation (24) suggests that the fine structure of $\mathcal{E}(2\tau)$ is totally described by $\langle E(2\tau)\rangle$, whereas its decay is given by $\mathcal{E}_{\mathrm{SC}}(2\tau)$. Important to us is the question whether the decay destroys any information on the spectrum of contact HFI, enclosed in $\langle E(2\tau)\rangle$, i.e., in $\langle E_c(2\tau)\rangle$. The answer is found from Fig. 3(a), indicating that $F_c(\tau)$ almost
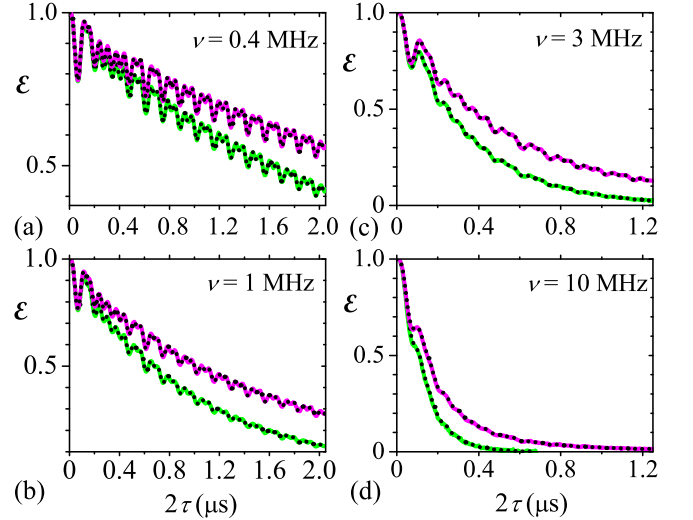

FIG. 6: (Color online) The decay of echo modulation for slow polaron hopping, $\eta \equiv \nu/\omega_{\mathrm{hf}} \ll 1$. The right-hand sides of Eq. (24) are plotted for $\alpha \equiv T/T_0 \gg 1$ (green), and $\alpha = 2$ (magenta). The corresponding left-hand sides are plotted with black dotted lines. The hopping attempt frequencies and corresponding values of η are: $\nu = 0.4$ MHz, $\eta = 0.0085$ (a), $\nu = 1$ MHz, $\eta = 0.021$ (b), $\nu = 3$ MHz, $\eta = 0.063$ (c), and $\nu = 10$ MHz, $\eta = 0.21$ (d). The plots clearly confirm the validity of Eq. (24).

disappears for $\tau > 1\,\mu$s. Thus, one is able to capture the complete spectrum if $\mathcal{E}(2\tau)$ is detectable for $\tau \leq 1\,\mu$s. Assuming that $\mathcal{E}(2\tau) \geq 0.05\,\mathcal{E}(0)$ is the restriction for the observation time, we find that for $\alpha \to \infty$ the contact HFI spectrum is not distorted if $\nu \leq 1.5$ MHz. At the same time, from Fig. 3(a) one can see that $F_c(\tau)$ is essentially non-zero for $\tau \leq 0.5\,\mu$s, meaning that the basic spectral features are detectable for $\nu \leq 3$ MHz.

For $\alpha \to \infty$ and larger ν the signal decay is faster and the spectrum distortion is progressively stronger. Furthermore, in the regime of fast hopping, $\eta \gg 1$, the fine structure of $\mathcal{E}(2\tau)$ is completely destroyed, even though the signal decays slower because of the motional narrowing. Instead of Eq. (24), here we get

$$\mathcal{E}(2\tau) = \mathcal{E}_{\mathrm{SC}}(2\tau). \qquad (25)$$

Therefore, for $\nu > 3$ MHz low-temperature (small-α) measurements can be crucial for the assessment of the primary ESEEM spectrum.

The experiment Ref. 14 confirms that the primary echo signal in MEH-PPV decays exponentially, for at least $T \geq 10$ K. This experiment does not address the fine structure of $\mathcal{E}(2\tau)$. However, the results of Ref. 14 suggest a uniform polaron hopping; $\alpha \gg 1$. At $T = 10$ K the hopping rate is estimated to be $\nu \approx 1.64$ MHz, whereas at $T = 295$ K it is $\nu \approx 2.87$ MHz. This refers to the slow hopping regime, where the ESEEM fine structure is shown to be observable.

B. Stimulated ESEEM of hopping polarons

The stimulated ESEEM of an ensemble of hopping polarons, $\mathcal{E}(\tau, T)$, is treated in the same way. We introduce its semiclassical counterpart, $\mathcal{E}_{SC}(\tau, T)$, and determine its T-dependence. Unlike the above analysis, however, here we restrict ourselves to the hopping regime, $\eta < 1$, relevant for MEH-PPV.

In the high-temperature limit, $\alpha \to \infty$, we find the simple exponential decay,

$$\mathcal{E}_{SC}(\tau, T) = \mathcal{E}_{SC}(2\tau) \exp(-\nu T). \qquad (26)$$

For finite α this decay slows down and becomes non-exponential. Similar to the primary ESEEM, the fine structure of the stimulated ESEEM is accurately described by the relation,

$$\mathcal{E}(\tau, T) = \langle E(\tau, T)\rangle \mathcal{E}_{SC}(\tau, T), \qquad (27)$$

with $\langle E(\tau, T)\rangle$ characterized in the previous Section.

The same question as to whether the decay destroys any information enclosed in $\langle E(\tau, T)\rangle$ on the contact HFI, i.e., in $\langle E_c(\tau, T)\rangle$, should be answered in this case. The question is relevant for stimulated ESEEM measurements aimed at the detection of the contact HFI, which imply $\tau = (\pi/\omega_I)n$ with even n. The answer is found from Eqs. (26), (27), and the fact that the amplitude of $\langle E_c(\tau_n, T)\rangle$ is very small for $T > 0.5\,\mu$s and nearly vanishing for $T > 0.75\,\mu$s (see Appendix A). Assuming that the observation time is restricted by $\mathcal{E}(\tau_n, T) \geq 0.05\,\mathcal{E}(\tau_n, 0)$, for $\alpha \gg 1$ the complete contact HFI spectrum of the stimulated ESEEM is detectable for $\nu \leq 4$ MHz, while its essential spectral features are preserved for $\nu \leq 6$ MHz. These limits are less restrictive than those on the primary ESEEM also because the decay of $\mathcal{E}_{SC}(\tau, T)$ with T is twice slower than that of $\mathcal{E}_{SC}(2\tau)$ with τ, cf. Eqs. (22) and (26).

Thus, in the absence of hopping, when the coherence of individual polaron and nuclear spins is retained, the total time-domain signal decays because of the orientational disorder (Sec. IV). The functions F_c and F_d, as introduced in Eqs. (17) and (18), describe the corresponding decrease of the signal. However, the spectral analysis still provides convenient means for probing the system, since the spectra remain undistorted. The distortion happens only when the coherence between polaron and the proton spins is reduced. This reduction happens primarily due to the polaron hopping, and in the situation of very slow polaron motion, the spectra remain reasonably undistorted.

Generally, the polarons undergoing multiple hops during an experimental run do not contribute in the ESEEM spectrum. The regimes where the spectrum is not distorted are characterized by a slow polaron motion. The polaron hopping destroys the coherence between the polaron and nuclear spins; already a single hop of the polaron destroys this coherence, and the signal from that individual polaron vanishes (the only exception is the case when the hop occurs either right after initial pulse or right before the final echo detection). As a result, the contribution of the polarons undergoing multiple hops is almost completely suppressed. The ESEEM signal can be detected when only a few hops occur, or no hops at all. Thus, our use of the multiple trapping model is justified by the physics of the problem, capturing the most important phenomena occurring in experiments. Based on these arguments we expect that using the multiple hopping or other transport models instead of the multiple trapping model will have only marginal consequences.

VI. CONCLUDING REMARKS

We have studied the ESEEM spectroscopy of the polarons in organic semiconductors, focusing on the experimentally relevant example of the π-conjugated polymer MEH-PPV. We use the microscopic picture of the polaron orbital state derived from earlier experiments.[24–26] Our study incorporates the random orientations of polymer chains and the polaron random hopping. The resulting ESEEM spectra demonstrate features caused by the interaction of the polaron spin with different groups of protons. In particular, for the stimulated ESEEM experiments we formulate a method that allows separate observation of the distant protons (coupled to the polaron spin via long-range dipolar interactions) and the nearby protons (coupled to the polaron via contact HFI).

Electrical or optical detection of any magnetic resonance relies upon the phenomenon of spin-dependent charge carrier recombination and transport. Since the work of Kaplan, Solomon, and Mott,[50] this phenomenon in commonly explained in terms of weakly coupled polaron spin pairs. Correspondingly, the pEDMR based ESEEM studies should take into account the weak coupling between the spins of different polarons. The perturbatively established effect of such a coupling on ESEEM spectra[51] results in the partial shifts of modulation frequencies $\delta\omega_\pm \approx \pm (J + D)^2/\omega_I$, where J and D are the strengths of the polaron pair spin exchange and dipolar coupling, respectively. In the case of MEH-PPV it is reasonable to neglect the spin exchange. The dipolar coupling can be neglected if $D^2/\omega_I \ll \omega_I$. This condition is met for the polaron separation greater than 2 nm. We neglected the effect of polaron-polaron spin coupling, assuming such large inter-polaron distances.

In a conventional ESR experiment the echo modulation decays due to the electron-nuclear, spin-lattice, and dipole-dipole interactions. In addition, in the pulse ODMR and EDMR experiments on organic semiconductors various recombination-dissociation processes can contribute to the ESEEM decay. However, the decay timescales measured so far[10,14,16] show that the polaron hopping constitutes the fastest channel of decay. We address the destructive effect of the polaron hopping and determine the hopping regimes where the ESEEM spectral features are not distorted. Based on the experiment

of Ref. 14 we conclude that the polaron hopping in MEH-PPV is within this regime and our approach is correct.

A pulse EDMR study of the stimulated ESEEM spectrum of polarons in MEH-PPV[15] reports the observation of a single spectral peak at about 14.5 MHz in regular MEH-PPV and two peaks at 2.2 MHz and 14.5 MHz in deuterated MEH-PPV. The ESEEM sidebands are not observed in either of these cases. Apparently, the working point in Ref. 15 is close to $\tau = (\pi/\omega_I)n$ with $n = 3$, where the signal of the nearby protons is suppressed, and the spectral peak originating from the distant protons is dominant. We believe that by choosing the parameters as proposed above it is possible to measure the spectrum of the nearby protons using the same experimental settings. Moreover, the theory can be straightforwardly generalized to other organic semiconductors.

Acknowledgments

Appendix A

In this Appendix we describe the details of the theoretical framework for the analysis in Section IV. Particularly, we address the disorder-averaged time-domain modulation signals $\langle E(2\tau)\rangle$, $\langle E(\tau,T)\rangle$, and their spectral functions, $\tilde{E}(\omega)$ and $\tilde{E}(\tau,\omega)$, in line with Ref. 20.

In real experiments, as well as during numerical simulations, time-domain signals are found at discrete values of time. Typically, one obtains an array of values, $f(t_k)$, for equidistant time points, $t_k = k\Delta t$, $k = 0, 1, .., L$. For the spectral analysis of such a signal it is convenient to introduce the discrete cosine Fourier transform, $\mathcal{F}_t[f(t)](\omega) \equiv \tilde{f}(\omega)$, as

$$\tilde{f}(\omega_j) = \sum_{k=0}^{L} 2f(t_k)\cos(\omega_j t_k) - f(t_0) + f(t_L), \quad \text{(A1)}$$

where $\omega_j = j\Delta\omega$ with $\Delta\omega = 2\pi/(\Delta t[L + 1])$ and integer j, while the last two terms are included to ensure a zero background. Because of the symmetry, $\tilde{f}(\omega_j) = \tilde{f}(2\pi/\Delta t - \omega_j)$, it is appropriate to confine $0 \le j \le L/2$, restricting the frequency domain to $0 \le \omega < \pi/\Delta t$. Without going into the details we assume Δt small enough to cover the necessary frequencies, and L large enough to ensure small frequency steps. Then one can regard $\tilde{f}$ as a function of continuous ω. This
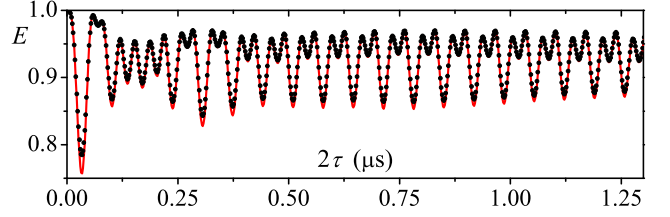

FIG. 7: (Color online) Comparison of the polymer chain orientation disorder averaged exact relation Eq. (10) (black points) and approximation Eq. (A4) (red line).

defines the cosine Fourier transforms we employ for the spectral analysis of modulation signals:

$$\tilde{E}(\omega) = \mathcal{F}_\tau[\langle E(2\tau)\rangle], \quad \tilde{E}(\tau,\omega) = \mathcal{F}_T[\langle E(\tau,T)\rangle]. \quad \text{(A2)}$$

Direct numerical evaluation of modulation depths from Eq. (13) shows that, for all orientations of the polymer chains, the maximum modulation depth of the contact hyperfine protons is 0.05 and the maximum depth of the distant protons is 0.007 (recall that, for MEH–PPV, in Eqs. (10) and (11) the contact protons are labelled by the subscript, $1 \le j \le N_c$, where $N_c = 22$, and the distant protons are labelled by $N_c < j \le N$). This allows us to approximate the factors in Eqs. (10) and (11) with exponents. For the primary ESEEM one gets:

$$E(2\tau) = \exp\left[-\sum_{j=1}^{N} 2k_j \sin^2\left(\frac{\omega_{j+}\tau}{2}\right)\sin^2\left(\frac{\omega_{j-}\tau}{2}\right)\right]. \quad \text{(A3)}$$

To some extent, the argument in Eq. (A3) is characterized by the sum of all depths, $\kappa = \sum_{j=1}^{N} k_j$. With the polymer orientation, κ varies between 0.03 and 0.242, and averages at about 0.136. The contribution of distant protons in this sum, $\kappa_d = \sum_{j>N_c} k_j$, is less than 0.06, with the average over the orientation disorder, $\langle \kappa_d \rangle = 0.047$. Dominant in κ is the contribution of contact hyperfine protons, $\kappa_c = \sum_{j=1}^{N_c} k_j$, which has a maximum of 0.2 and averages at about 0.089. However, the contact hyperfine protons have a large dispersion of modulation frequencies, and even relatively large fluctuations of κ_c do not generate a large argument in Eq. (A3). Therefore it is reasonable to expand the exponent (A3) and write:

$$E(2\tau) \approx 1 - \sum_{j=1}^{N} 2k_j \sin^2\left(\frac{\omega_{j+}\tau}{2}\right)\sin^2\left(\frac{\omega_{j-}\tau}{2}\right). \quad \text{(A4)}$$

This approximation is further reinforced by averaging Eqs. (10) and (A4) over orientation disorder numerically and comparing the results in Fig. 7. After a simple transformation Eq. (A4) goes into Eq.(14) of the main text.

The approximation Eq. (15) in the main text for the distant protons is based on the fact that the polaron spin coupling to these protons is weak, $A_j, B_j \ll \omega_I$. The

following arguments substantiate the same approximation for the contact protons. From Eq. (12) it is seen that the approximation error is $\propto B_j^2/(\omega_I \pm A_j/2)$. Consistent with this, we numerically find the largest error, $\omega_{j+} - (\omega_I + A_j/2) \approx 0.1$ MHz, occurring for the largest B_j. It results for a C–H proton at vinyl site E, when the external magnetic field is parallel to $\hat{\mathbf{x}} + \hat{\mathbf{y}}$ in the principal axes at E (see Fig. 1). This error is about 1% of the corresponding frequency values, so the approximation is quite accurate.

The stimulated ESEEM is analyzed in a similar way. By virtue of small values of k_j, Eq. (11) is reduced to the sum Eq. (19) in the main text. After averaging over the disorder in polymer chain orientations and separating the contact and the distant proton contributions $\langle E_\beta(\tau, T)\rangle$, $\beta = d, c$, one gets

$$\langle E_\beta(\tau, T)\rangle = -\frac{1}{2}\kappa_\beta + \frac{1}{2}F_\beta(\tau)\cos\omega_I\tau$$
$$+\frac{1}{2}F_\beta(\tau + T)\cos\omega_I[\tau + T] \quad \text{(A5)}$$
$$-\frac{1}{4}F_\beta(T)\cos\omega_I[2\tau + T] - \frac{1}{4}F_\beta(2\tau + T)\cos\omega_I T,$$

from which Eq. (20) of the main text is written.

The T- dependence of $\langle E_d(\tau, T)\rangle$ is simple modulation with the frequency ω_I. To find its τ- dependence we rewrite the modulation part of Eq. (A5) as

$$\langle E_\beta(\tau, T)\rangle \simeq \frac{1}{2}\Lambda_\beta(\tau, T)\cos\big(\omega_I T + \varphi_\beta(\tau, T)\big), \quad \text{(A6)}$$

with $\varphi_\beta = \arg Z_\beta (\text{mod } \pi)$ and $\Lambda_\beta = Z_\beta e^{-i\varphi_\beta}$, where

$$Z_\beta = e^{i\omega_I\tau}F_\beta(\tau + T) - \frac{1}{2}e^{2i\omega_I\tau}F_\beta(T) - \frac{1}{2}F_\beta(2\tau + T). \quad \text{(A7)}$$

As defined, $\Lambda_d(\tau, T)$ and $\varphi_d(\tau, T)$ are smooth functions of T, varying insignificantly at times, $T \sim 1/\omega_I$. In contrast, their τ- dependence is abrupt, because of the presence of exponential factors in Eq. (A7). The largest and smallest values of $\Lambda_d(\tau, T)$ for a fixed T can be found in an adiabatic accuracy, by differentiating the fast exponents with respect to τ, while regarding the F_d factors as constants. It is in fact more convenient to use the relation, $\Lambda_d^2 = |Z_d|^2$, and differentiate $|Z_d|^2$. One gets:

$$\partial_\tau |Z_d|^2 \approx \omega_I \sin\omega_I\tau\big[F_d(\tau + T)F_d(2\tau + T) \quad \text{(A8)}$$
$$+F_d(T)F_d(\tau + T) - 2\cos\omega_I\tau F_d(T)F_d(2\tau + T)\big].$$

This yields minima at $\omega_I\tau_n = \pi n$ for even integer n and maxima at $\omega_I\tau_n = \pi n$ for odd integer n, as expected.

To visualize the modulation reduction, in Fig. 8 we plot $\Lambda_d(\tau_n, T)$ against T for $n = 1, .., 30$. We note that these τ_n include all possible critical values within the interval, $0 < \tau < 1\,\mu s$, which covers the experimentally available τ- domain, taking into account the decay of the signal in a real experiment. It is seen that for small n the reduction is more than two orders of magnitude, and for large n it is more than 15 times.
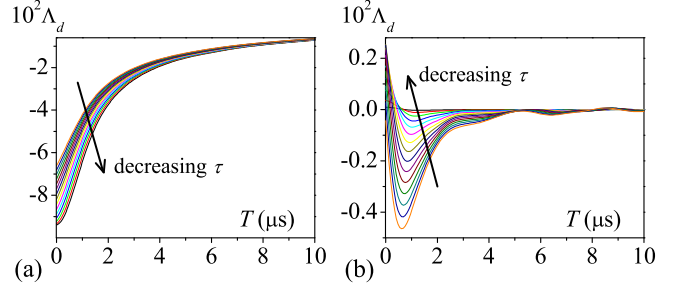

FIG. 8: (Color online) Plots of the amplitude, $\Lambda_d(\tau_n, T)$, versus T at fixed $\tau_n = (\pi/\omega_I)n$, for (a) odd $n = 1, 3, .., 29$, and (b) even $n = 2, 4, .., 30$. The plots demonstrate the reduction of $\Lambda_d(\tau_n, T)$ when going from odd to even n. For small n the decrease of $\Lambda_d(\tau_n, T)$ from odd to even n is more than two orders of magnitude. For large n it is more that 15 times.

For the contribution of contact hyperfine protons, $\langle E_c(\tau, T)\rangle$, the modulation given by Eqs. (A5) and (A6) cannot be interpreted as having a single frequency, because the function F_c, and therefore $\Lambda_c(\tau, T)$ and $\varphi_c(\tau, T)$, vary abruptly on the timescale, $T \sim 1/\omega_I$. Still, $\Lambda_c(\tau, T)$ gives the overall strength of this modulation and it is useful to inspect this quantity for the above critical values of τ. Figure 9 plots $\Lambda_c(\tau_n, T)$ versus T for the first 20 values of τ_n. Overall, the magnitudes of $\Lambda_c(\tau_n, T)$ in Fig. 9 are close to each other for even and odd n, meaning that there is no particular reduction of the corresponding modulation. From Fig. 9 we also infer that $\Lambda_c(\tau_n, T)$, and therefore $\langle E_c(\tau_n, T)\rangle$, is very small for $T > 0.5\,\mu s$, and nearly vanishes for $T > 0.75\,\mu s$.

Appendix B

In this Appendix we outline the generalization of Eqs. (10), (11) for an ensemble of polarons hopping over the polymer sites of random orientations. Consider pulse
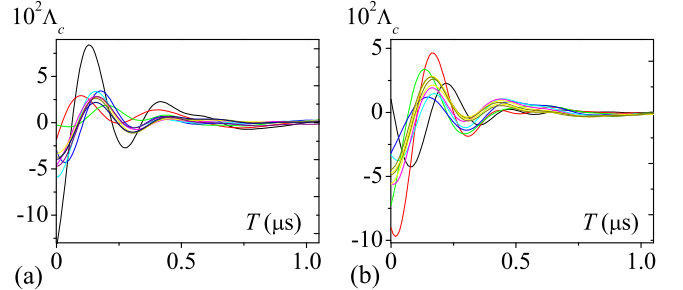

FIG. 9: (Color online) The amplitude, $\Lambda_c(\tau_n, T)$, is plotted versus T at fixed $\tau_n = (\pi/\omega_I)n$, for (a) odd $n = 1, .., 19$, and (b) even $n = 2, .., 20$. Though the individual curves are not well resolved, it is seen that there is no notable difference in the orders of magnitude of $\Lambda_c(\tau_n, T)$ with even and odd n.

sequences similar to those in Fig. 2(a), but with unequal delay times; $\pi/2$ - τ_1 - π - τ_2 - *echo*, and $\pi/2$ - τ_1 - $\pi/2$ - T - $\pi/2$ - τ_2 - *echo*. Using the density matrix formalism, the modulation functions are

$$E(\tau_1, \tau_2) = \mathcal{N}\,\mathrm{Tr}\left[U(\tau_1, \tau_2)\hat{\rho}(0)U^\dagger(\tau_1, \tau_2)S^y\right], \quad \text{(B1)}$$

$$E(\tau_1, T, \tau_2) = \mathcal{N}\,\mathrm{Tr}\left[U(\tau_1, T, \tau_2)\hat{\rho}(0)U^\dagger(\tau_1, T, \tau_2)S^y\right],$$

where $\hat{\rho}(0) \propto (1/2 + S^z)$ is the initial density operator introduced in Eq. (8) and $\mathcal{N}^{-1} = \mathrm{Tr}\left([3\pi/2]\hat{\rho}(0)[3\pi/2]^\dagger S^y\right)$ is the normalization factor. The evolution operators are given by

$$U(\tau_1, \tau_2) = e^{-i\tau_2\tilde{H}}[\pi]e^{-i\tau_1\tilde{H}}[\pi/2], \quad \text{(B2)}$$

$$U(\tau_1, T, \tau_2) = e^{-i\tau_2\tilde{H}}[\pi/2]e^{-iT\tilde{H}}[\pi/2]e^{-i\tau_1\tilde{H}}[\pi/2],$$

where $\tilde{H}$ is the Hamiltonian (1) in the coordinate system rotating around $\hat{\mathbf{z}}$ with the frequency Ω. For later reference, we also consider the free induction decay,

$$F(t) = -\mathcal{N}\,\mathrm{Tr}\left[e^{-it\tilde{H}}[\pi/2]\hat{\rho}(0)[\pi/2]^\dagger e^{it\tilde{H}}S^y\right]. \quad \text{(B3)}$$

By taking the traces over the polaron spin space, Eqs. (B1), (B3) are reduced to the nuclear spin traces, involving the nuclear spin Hamiltonians,

$$h^\pm = \pm\frac{1}{2}\sum_{j=1}^{N}\left(A_j I_j^z + B_j I_j^x\right) - \sum_{j=1}^{N}\omega_I I_j^z. \quad \text{(B4)}$$

Subsequently, the nuclear spin traces are calculated explicitly. More specifically, we have:

$$F(t) = 2^{-N}\mathrm{Tr}_I\left[e^{-ith^-}e^{ith^+}\right] = \prod_{j=1}^{N}f_j(t), \tag{B5}$$

$$E(\tau_1, \tau_2) = 2^{-N}\mathrm{Tr}_I\left[e^{-i\tau_2 h^+}e^{-i\tau_1 h^-}e^{i\tau_1 h^+}e^{i\tau_2 h^-}\right] = \prod_{j=1}^{N}\epsilon_j(\tau_1, \tau_2), \tag{B6}$$

$$E(\tau_1, T, \tau_2) = 2^{-N-1}\mathrm{Tr}_I\left[e^{-i(\tau_2+T)h^+}e^{-i\tau_1 h^-}e^{i(\tau_1+T)h^+}e^{i\tau_2 h^-}\right] + \left(+\leftrightarrow-\right)^* = \frac{1}{2}\prod_{j=1}^{N}\epsilon_j^+(\tau_1, T, \tau_2) + \left(+\leftrightarrow-\right)^*, \tag{B7}$$

where $(+\leftrightarrow-)^*$ denote the complex conjugates of previous expressions with the superscripts swapped, and the functions

$$f_j(t) = \cos\frac{\omega_{j+}t}{2}\cos\frac{\omega_{j-}t}{2} + \frac{\omega_I^2 - A_j^2/4 - B_j^2/4}{\omega_{j+}\omega_{j-}}\sin\frac{\omega_{j+}t}{2}\sin\frac{\omega_{j-}t}{2}, \tag{B8}$$

$$\epsilon_j(t_1, t_2) = f_j(t_1 - t_2) - 2k_j\sin\frac{\omega_{j+}t_1}{2}\sin\frac{\omega_{j-}t_1}{2}\sin\frac{\omega_{j+}t_2}{2}\sin\frac{\omega_{j-}t_2}{2},$$

$$\epsilon_j^\pm(t_1, T, t_2) = f_j(t_1 - t_2) - 2k_j\sin\frac{\omega_{j\pm}(t_1+T)}{2}\sin\frac{\omega_{j\pm}(t_2+T)}{2}\sin\frac{\omega_{j\mp}t_1}{2}\sin\frac{\omega_{j\mp}t_2}{2},$$

are introduced, with $\omega_{j\pm}$ and k_j given in Eqs. (12), (13).

To generalize Eqs. (B5) for hopping polarons, consider a polaron random walk right after the initial $\pi/2$-pulse (time $t = 0$) from some polymer site, $\mathbf{r}_0$. Its trajectory, $\mathbf{R}(t)$, specifies the waiting time, δt_n, which the polaron spends at $\mathbf{r}_n$. Other necessary details of $\mathbf{R}(t)$ are represented in Fig. 10(a), showing that for time t the polaron performes M hops, arriving in the site $\mathbf{r}_M$ time $\delta t'_M$ before the detection. The prime indicates that $\delta t'_M$ is not the total waiting time at $\mathbf{r}_M$. By this definition,

$$t = \delta t'_M + \sum_{n=0}^{M-1}\delta t_n, \qquad \delta t_M = \delta t'_M + \delta t''_M, \quad \text{(B9)}$$

The free induction decay of a polaron undergoing such a random walk is given by

$$F_{\mathbf{R}}(t) = 2^{1-N(M+1)}\,\mathrm{Tr}\left[u_{\mathbf{R}}(t)S^y u_{\mathbf{R}}^\dagger(t)S^y\right], \quad \text{(B10)}$$

with the time-ordered operator $u_{\mathbf{R}}(t)$, replacing the exponential factors in Eq. (B3),

$$u_{\mathbf{R}}(t) = e^{-i\delta t'_M H_M}\overleftarrow{\prod_{n=0}^{M-1}}e^{-i\delta t_n H_n}. \quad \text{(B11)}$$

Here the arrow indicates the inverse order of factors in the products. The transient Hamiltonians in Eq. (B11)

are

$$H_n = \sum_{j=1}^{N} S^z\big(A_{j,\mathbf{r}_n} I^z_{j,\mathbf{r}_n} + B_{j,\mathbf{r}_n} I^x_{j,\mathbf{r}_n}\big) - \sum_{l=0}^{M}\sum_{j=1}^{N} \omega_I I^z_{j,\mathbf{r}_l}, \quad \text{(B12)}$$

where $\mathbf{I}_{j,\mathbf{r}}$ is the spin operator and $A_{j,\mathbf{r}}$, $B_{j,\mathbf{r}}$ are the hyperfine coupling constants of the j-th proton located at site $\mathbf{r}$, and the sum over l includes all $M+1$ molecular sites visited for the random walk $\mathbf{R}(t)$. The time dependence of the spin Hamiltonian is thus incorporated in the first term of Eq. (B12), describing the hyperfine coupling of the polaron spin with protons near the site, $\mathbf{r}_n = \mathbf{R}(t)$, occupied by the polaron at time t.

The trace over the polaron spin space in Eq. (B10) can be easily taken as the transient Hamiltonians (B12) conserve S^z. The result is written in terms of the trace over the nuclear spins:

$$F_{\mathbf{R}}(t) = 2^{-N(M+1)}\mathrm{Tr}_I\Big[u_{\mathbf{R},-}(t)u^\dagger_{\mathbf{R},+}(t)\Big]. \quad \text{(B13)}$$

where we have introduced

$$u_{\mathbf{R},\pm}(t) = e^{-i\delta t'_M h^\pm_M} \overleftarrow{\prod_{n=0}^{M-1}} e^{-i\delta t_n h^\pm_n}. \quad \text{(B14)}$$

The spin Hamiltonians, $h^\pm_n$, are given by Eq. (B4), with the coupling constants and spin operators of protons at $\mathbf{r}_n$. Note that unlike Eq. (B12), the last term in Eq. (B4) involves nuclear spin operators only for a single site. This simplification is general for transport models neglecting the polaron returns to the sites visited previously, such as the multiple trapping model adopted in this study. Moreover, neglecting the polaron returns allows to calculate the trace in Eq. (B13) explicitly. One finds:

$$F_{\mathbf{R}}(t) = \left(\prod_{n=0}^{M-1} F_n(\delta t_n)\right) F_M(\delta t'_M), \quad \text{(B15)}$$

where $F_n(t)$ is the free induction decay Eq. (B5) calculated for the single site, $\mathbf{r}_n$.

Similar expressions can be written for the primary and stimulated ESE modulation functions, provided the polaron random walk trajectory is specified relative to the
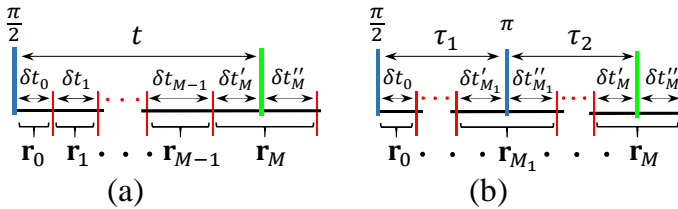

FIG. 10: (Color online) Schematic definitions of polaron random walk trajectories, $\mathbf{R}(t)$, for free induction decay (a), and primary echo (b). The blue lines denote the pulses. The green lines show the detection points. The red bars are polaron random hops.
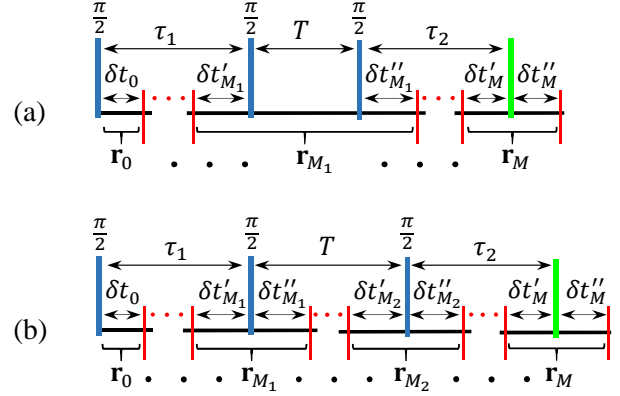

FIG. 11: (Color online) Illustration of notations for polaron random walk trajectories during the stimulated pulse sequence. The blue bars symbolize the pulses. The green bars show the detection. The red lines are polaron random hops. (a) Trajectories of type $\mathbf{R}_0$, Eq. (B17); no polaron hop occurs in the time interval T. (b) Trajectories of type $\mathbf{R}_1$, Eq. (B17); at least one hop occurs in the time interval T.

pulse sequence. Namely, for the primary sequence let $\mathbf{R}(\tau_1+\tau_2) = \mathbf{r}_M$, and the instantaneous π-pulse is applied $\delta t'_{M_1}$ time after the polaron arrives in the site $\mathbf{r}_{M_1}$, and $\delta t''_{M_1}$ time before it makes the next hop, see Fig. 10(b). The primary ESE modulation from a spin with this trajectory is found to be

$$E_{\mathbf{R}}(\tau_1,\tau_2) = \left(\prod_{n=0}^{M_1-1} F_n(\delta t_n)\right) E_{M_1}(\delta t'_{M_1}, \delta t''_{M_1}) \quad \text{(B16)}$$
$$\times \left(\prod_{n=M_1+1}^{M-1} F_n(\delta t_n)\right) F_M(\delta t'_M),$$

where $E_n(t_1,t_2)$ is the modulation function (B6), for $\mathbf{r}_n$.

The stimulated ESE modulation critically depends on whether a random walk involves a hop in the interval T or not. We separate these cases in Fig. 11(a) and (b). The trajectories with no hops during the interval T, Fig. 11(a), are denoted by $\mathbf{R}_0$, while those incorporating hops in T, Fig. 11(b), by $\mathbf{R}_1$. With the further details of trajectories specified in Fig. 11, one gets:

$$E_{\mathbf{R}_0}(\tau_1,T,\tau_2) = \left(\prod_{n=0}^{M_1-1} F_n(\delta t_n)\right) E_{M_1}(\delta t'_{M_1}, T, \delta t''_{M_1})$$
$$\times \left(\prod_{n=M_1+1}^{M-1} F_n(\delta t_n)\right) F_M(\delta t'_M), \quad \text{(B17)}$$

where $E_n(t_1,T,t_2)$ is is given by Eq. (B7) at $\mathbf{r}_n$, and

$$E_{\mathbf{R}_1}(\tau_1,T,\tau_2) = \left(\prod_{n=0}^{M_1-1} F_n(\delta t_n)\right) F_{M_1}(\delta t'_{M_1})$$
$$\times F_{M_2}(\delta t''_{M_2})\left(\prod_{n=M_2+1}^{M-1} F_n(\delta t_n)\right) F_M(\delta t'_M). \quad \text{(B18)}$$

Finally, the free induction decay and the ESE modulations of the ensemble of randomly walking polarons is found from Eqs. (B15) – (B18), via averaging over the random-walk trajectories:

$$\mathcal{F}(t) = \langle F_{\mathbf{R}}(t)\rangle_{\{\mathbf{R}\}}, \tag{B19}$$

$$\mathcal{E}(\tau_1, \tau_2) = \langle E_{\mathbf{R}}(\tau_1, \tau_2)\rangle_{\{\mathbf{R}\}}, \tag{B20}$$

$$\mathcal{E}(\tau_1, T, \tau_2) = \langle E_{\mathbf{R}}(\tau_1, T, \tau_2)\rangle_{\{\mathbf{R}\}}. \tag{B21}$$

The averages are evaluated numerically, by a Monte Carlo sampling of random walk trajectories, including the random on-site trapping energies defining the waiting time statistics via Eq. (21). In our simulations we also incorporate the random orientations of polymer chains.

Appendix C

In this Appendix we investigate $\mathcal{F}(t)$, $\mathcal{E}(\tau_1, \tau_2)$, and $\mathcal{E}(\tau_1, T, \tau_2)$ analytically, within the multiple trapping model at $\alpha \to \infty$. This implies uniform hopping rates, $W_{\mathbf{r}} = \nu$, entailing the Poissonian waiting time distribution, $P(\delta t) = \nu \exp(-\nu \delta t)$. In this limit the free induction decay obeys the Dyson-type integral equation,[42,52]

$$\mathcal{F}(t) = g(t)e^{-\nu t} + \nu \int_0^t dt' e^{-\nu t'} g(t')\mathcal{F}(t - t'), \tag{C1}$$

where the on-site relaxation function,

$$g(t) = \langle F(t)\rangle, \tag{C2}$$

is introduced. Here, $F(t)$ is given by Eq. (B5), and the brackets mean the average over random orientations of molecular sites. In Eq. (C1) the first term is the relaxation if for time t the polarons do not hop, which occurs with the probability $e^{-\nu t}$, and the integral accounts for the relaxation with the first hop happening at time $t' < t$.

The formal solution of Eq. (C1) is given in terms of the Laplace transform:

$$\tilde{\mathcal{F}}(s) = \frac{\tilde{g}(s + \nu)}{1 - \nu\tilde{g}(s + \nu)}, \tag{C3}$$

where $\tilde{f}(s) = \int_0^\infty \exp(-st)f(t)dt$ denotes the Laplace transform of $f(t)$. However, from this equation $\mathcal{F}(t)$ can be found only numerically, as the inverse Laplace transform of Eq. (C3) is not accessible analytically.

Semiclassical description

A semiclassical approximation for $\mathcal{F}$ and $\mathcal{E}$ follows upon replacing the Hamiltonian in Eqs. (B2), (B3) by its semiclassical counterpart, Eq. (7). The resulting on-site free induction decay has the simple form,

$$g_0(t) = \langle\cos(\omega_z t)\rangle_{\omega_z} = \exp(-\omega_{\mathrm{hf}}^2 t^2/2). \tag{C4}$$

Still, the solution for the semiclassical free induction decay, $\mathcal{F}_0(t)$, using the inverse Laplace transform (C3), can be found only numerically.[52]

In what follows we give a perturbative treatment for the semiclassical echo modulation functions, $\mathcal{E}_{\mathrm{SC}}(2\tau) = \mathcal{E}(\tau, \tau)$ and $\mathcal{E}_{\mathrm{SC}}(\tau, T) = \mathcal{E}(\tau, T, \tau)$, from which Eqs. (22) and (26) of the main text result. In the semiclassical approximation and within the multiple trapping model at $\alpha \to \infty$, Eqs. (B19) – (B21) are related as

$$\mathcal{E}_{\mathrm{SC}}(2\tau) = e^{-2\nu\tau}\left[1 + 2\nu \int_0^\tau e^{2\nu t}\mathcal{F}_0^2(t)dt\right], \tag{C5}$$

$$\mathcal{E}_{\mathrm{SC}}(\tau, T) = e^{-\nu T}\mathcal{E}_{\mathrm{SC}}(2\tau) + \mathcal{F}_0^2(\tau)\left(1 - e^{-\nu T}\right), \tag{C6}$$

detailed derivation of which will be given elsewhere.[53] Thus, $\mathcal{E}_{\mathrm{SC}}(2\tau)$ and $\mathcal{E}_{\mathrm{SC}}(\tau, T)$ are determined by $\mathcal{F}_0(t)$. Note that the first term in Eq. (C6) is the contribution of type $\mathbf{R}_0$ trajectories, Fig. 11(a), while the last term is that of the type $\mathbf{R}_1$ trajectories, Fig. 11(b).

In the regime of slow hopping, $\eta \equiv \nu/\omega_{\mathrm{hf}} \ll 1$, a reasonably good approximation can be made for $\mathcal{F}_0(t)$ from Eq. (C1) iteratively. To the linear order in η one gets:

$$\mathcal{F}_0(t) = e^{-\nu t}\left[g_0(t) + \nu \int_0^t dt' g_0(t')g_0(t - t')\right]. \tag{C7}$$

Using this in Eq. (C5) leads to Eq. (22) in the main text. Equation (C7) also shows that the decay of $\mathcal{F}_0(t)$ is nearly Gaussian and fast, so that for $\tau > 1/\omega_{\mathrm{hf}}$ the last term in Eq. (C6) can be neglected, and Eq. (26) in the main text can be written.

In the fast hopping regime, $\eta \gg 1$, the Laplace transform appears to be useful. One has:

$$\mathcal{F}_0(t) = \frac{1}{2\pi i}\int_{-i\infty}^{i\infty} ds\, e^{st}\tilde{\mathcal{F}}_0(s), \tag{C8}$$

with $\tilde{\mathcal{F}}_0(s)$ given by Eq. (C3) and the Laplace transform,

$$\tilde{g}_0(s) = \sqrt{\pi/2}\,\omega_{\mathrm{hf}}^{-1}\exp\left(s^2/2\omega_{\mathrm{hf}}^2\right)\mathrm{erfc}\left(s/\sqrt{2}\omega_{\mathrm{hf}}\right), \tag{C9}$$

where $\mathrm{erfc}(x)$ is the complementary error function. $\tilde{\mathcal{F}}_0(s)$ is holomorphic on the complex half-plane, $\mathrm{Re}(s) < 0$, excluding the simple poles determined by the denominator of Eq. (C3). A thorough analysis of the inverse Laplace transform (C8) shows that $\tilde{\mathcal{F}}_0(s)$ has one real negative pole, s_0, and infinitely many complex poles.[53] Also, for $\eta \gg 1$ the contribution of s_0 dominates in the integral (C8), giving $\mathcal{F}_0(t) = -(\omega_{\mathrm{hf}}^2/\nu s_0)\exp(s_0 t)$. From the large-argument asymptote of Eq. (C9) one finds $s_0 = -\omega_{\mathrm{hf}}^2/\nu$, leading to the well-known result in the motional narrowing regime, $\mathcal{F}_0(t) = \exp(-\omega_{\mathrm{hf}}^2 t/\nu)$. With this $\mathcal{F}_0(t)$, the integral term in Eq. (C5) is dominant, yielding $\mathcal{E}_{\mathrm{SC}}(2\tau) = \exp(-2\,\omega_{\mathrm{hf}}^2\tau/\nu)$.

* Current address: QuTech and Kavli Institute of Nanoscience, TU Delft, Lorentzweg 1, 2628 CJ Delft, the Netherlands

[1] S. R. Forrest, Nature (London) **428**, 911 (2004).

[2] Special issue on organic electronics and optoelectronics. Chem. Rev. **107**, 923 (2007).

[3] J. Shinar, Laser Photonics Rev. **6**, 767 (2012).

[4] B. C. Cavenett, Adv. Phys. **30**, 475 (1981).

[5] R. A. Street, Phys. Rev. B **26**, 3588 (1982).

[6] S. Depinna, B. C. Cavenett, I. G. Austin, T. M. Searle, M. J. Thompson, J. Allison, and P. G. L. Comberd, Philos. Mag. B **46**, 473 (1982).

[7] M. Stutzmann, M. S. Brandt, and M. W. Bayerl, J. Non-Cryst. Solids **266 269**, 22 (2000).

[8] E. Lifshitz, L. Fradkin, A. Glozman, and L. Langof, Annu. Rev. Phys. Chem. **55**, 509 (2004).

[9] D. R. McCamey, H. Huebl, M. S. Brandt, W. D. Hutchison, J. C. McCallum, R. G. Clark, and A. R. Hamilton, Appl. Phys. Lett. **89**, 182115 (2006).

[10] D. R. McCamey, H. A. Seipel, S.-Y. Paik, M. J. Walter, N. J. Borys, J. M. Lupton, and C. Boehme, Nat. Mater. **7**, 723 (2008).

[11] D. R. McCamey, K. J. van Schooten, W. J. Baker, S.-Y. Lee, S.-Y. Paik, J. M. Lupton, and C. Boehme, Phys. Rev. Lett. **104**, 017601 (2010).

[12] D. R. McCamey, S.-Y. Lee, S.-Y. Paik, J. M. Lupton, and C. Boehme, Phys. Rev. B **82**, 125206 (2010).

[13] J. Behrends, A. Schnegg, K. Lips, E. A. Thomsen, A. K. Pandey, I. D. W. Samuel, and D. J. Keeble, Phys. Rev. Lett. **105**, 176601 (2010).

[14] W. J. Baker, T. L. Keevers, J. M. Lupton, D. R. McCamey, and C. Boehme, Phys. Rev. Lett. **108**, 267601 (2012).

[15] H. Malissa, M. Kavand, D. P. Waters, K. J. van Schooten, P. L. Burn, Z. V. Vardeny, B. Saam, J. M. Lupton, and C. Boehme, Science **345**, 1487 (2014).

[16] K. J. van Schooten, D. L. Baird, M. E. Limes, J. M. Lupton, and C. Boehme, Nat. Commun. **6**, 6688 (2015).

[17] C. P. Slichter, *Principles of Magnetic Resonance* (Harper & Row, New York, 1963).

[18] V. A. Dediu, L. E. Hueso, I. Bergenti, and C. Taliani, Nat. Mater. **8**, 850 (2009).

[19] T. Nguyen, G. Hukic-Markosian, F. Wang, L. Wojcik, X. Li, E. Ehrenfreund, Z. Vardeny, Nat. Mater. **9**, 345 (2010).

[20] S. A. Dikanov and Y. D. Tsvetkov, *Electron Spin Echo Envelope Modulation (ESEEM) spectroscopy* (CRC Press, Boca Raton, FL, 1992).

[21] A. Schweiger and G. Jeschke, *Principles of Pulsed Electron Paramagnetic Resonance* (Oxford University Press, Oxford, UK, 2001).

[22] K. Schulten and P. G. Wolynes, J. Chem. Phys. **68**, 3292 (1978).

[23] A. Abragam, *Principles of Nuclear Magnetism* (Oxford University Press, New York, 1961).

[24] S. Kuroda, T. Noguchi, and T. Ohnishi, Phys. Rev. Lett. **72**, 286 (1994).

[25] S. Kuroda, K. Murata, T. Noguchi, and T. Ohnishi, J. Phys. Soc. Jpn. **64**, 1363 (1995).

[26] S. Kuroda, K. Marumoto, H. Ito, N. C. Greenham, R. H. Friend, Y. Shimoi, and S. Abe, Chem. Phys. Lett. **325**, 183 (2000).

[27] Y. Shimoi, S. Abe, S. Kuroda, and K. Murata, Solid State Commun. **95**, 137 (1995).

[28] S. Kuroda, Appl. Magn. Reson. **23**, 455 (2003).

[29] J. R. Morton, Chem. Rev. **64**, 453 (1964).

[30] L. Claes, J. P. Francois, and M. S. Deleuze, Chem. Phys. Lett. **339**, 216 (2001).

[31] S. Kilina, N. Dandu, E. R. Batista, A. Saxena, R. L. Martin, D. L. Smith, and S. Tretiak, J. Phys. Chem. Lett. **4**, 1453 (2013).

[32] T. Qin and A. Troisi, J. Am. Chem. Soc. **135**, 11247 (2013).

[33] A. Bondi, J. Phys. Chem. **68**, 441 (1964).

[34] I. Motoc and G. R. Marshall, Chem. Phys. Lett. **116**, 415 (1985).

[35] W. J. Spillane, G. G. Birch, M. G. B. Drew, and I. Bartolo, J. Chem. Soc., Perkin Trans. **2**, 497 (1992).

[36] Throughout the paper, by the Fourier transform of a function of two variables, (τ, T), we mean the transformation over the variable T, whereas τ is kept as a parameter. For the precise definition of these Fourier transforms see Appendix A.

[37] The largest value of $|A_j|$ within the HFI under consideration is about $2\pi \times 9.4$ MHz, whereas the X – band proton Larmor frequency is about $\omega_I = 2\pi \times 14.7$ MHz.

[38] V. V. Mkhitaryan and V. V. Dobrovitski, Phys. Rev. B **92**, 054204 (2015).

[39] R. C. Roundy and M. E. Raikh, Phys. Rev. B **90**, 201203 (2014).

[40] R. Czech and K. W. Kehr, Phys. Rev. Lett. **53**, 1783 (1984); Phys. Rev. B **34**, 261 (1986).

[41] P. Mitra and P. Le Doussal Phys. Rev. B **44**, 12035 (1991).

[42] R. S. Hayano, Y. J. Uemura, J. Imazato, N. Nishida, T. Yamazaki, and R. Kubo, Phys. Rev. B **20**, 850 (1979).

[43] A. Jakobs and K. W. Kehr, Phys. Rev. B **48**, 8780 (1993).

[44] B. Hartenstein, H. Bassler, A. Jakobs, and K. W. Kehr, Phys. Rev. B **54**, 8574 (1996).

[45] N. J. Harmon and M. E. Flatté, Phys. Rev. Lett. **110**, 176602 (2013).

[46] N. J. Harmon and M. E. Flatté, Phys. Rev. B **90**, 115203 (2014).

[47] V. Coropceanu, J. Cornil, D. A. da Silva Filho, Y. Olivier, R. Silbey, and J.-L. L. Brèdas, Chem. Rev. **107**, 926 (2007).

[48] P. W. M. Blom and M. C. J. M. Vissenberg, Mater. Sci. Eng., R **27**, 53 (2000).

[49] Z. Yue, V. V. Mkhitaryan, and M. E. Raikh, arXiv: 1602.00785.

[50] D. Kaplan, I. Solomon, and N. F. Mott, J. Phys. (Paris) **39**, L51 (1978).

[51] G. Zwanenburg and P. J. Hore, J. Magn. Reson. A **114**, 139 (1995).

[52] G. Allodi and R. De Renzi, Phys. Scr. **89**, 115201 (2014).

[53] V. V. Mkhitaryan and V. V. Dobrovitski, unpublished.